

Submitted to: ApJ Version: October 31, 2018

Synthesis of intermediate-mass elements in classical novae: from Si to Ca

Jordi José

Departament de Física i Enginyeria Nuclear (UPC), Av. Víctor Balaguer, s/n, E-08800 Vilanova i la Geltrú (Barcelona), SPAIN

and

Institut d'Estudis Espacials de Catalunya, Edifici Nexus-201, C/ Gran Capità 2-4, E-08034 Barcelona, SPAIN

Alain Coc

Centre de Spectrométrie Nucléaire et de Spectrométrie de Masse, IN2P3-CNRS, Université Paris Sud, Bât.104, F-91405 Orsay Campus, FRANCE

and

Margarita Hernanz

Instituto de Ciencias del Espacio (CSIC), and

Institut d'Estudis Espacials de Catalunya, Edifici Nexus-201, C/ Gran Capità 2-4, E-08034 Barcelona, SPAIN

ABSTRACT

Thermonuclear runaways driven by accretion into degenerate white dwarf cores are the source that power classical nova outbursts. In this paper, we identify the dominant nuclear paths involved in the synthesis of intermediate-mass elements, from Si to Ca, during such violent events. New evolutionary sequences of $1.35 M_{\odot}$ ONe novae have been computed, using updated nuclear reaction rates. The main nuclear activity in this region is powered by the leakage from the NeNa–MgAl region, where the activity is confined during the early stages of the explosion. We discuss the critical role played by $^{30}\text{P}(p,\gamma)$ in the synthesis of nuclear species beyond sulfur and point out the large uncertainty that affects its rate, which has dramatic consequences for studies of nova nucleosynthesis in the Si–Ca mass region.

Subject headings: novae, cataclysmic variables — nuclear reactions, nucleosynthesis, abundances

1. Introduction

Classical novae inject nuclear processed material into the interstellar medium, and therefore may play a role in the Galactic nucleosynthesis. Isotopes likely attributed to nova outbursts include ^{13}C , ^{15}N and ^{17}O (see José & Hernanz 1998, and references therein). Current hydrodynamic models of classical novae show that explosions on carbon-oxygen white dwarfs (hereafter, CO novae) are dominated by the synthesis of CNO-group nuclei, largely overproduced in the ejecta with respect to solar abundances (Starrfield et al. 1997; Kovetz & Prialnik 1997; José & Hernanz 1998). On the other hand, explosions on oxygen-neon white dwarfs (hereafter, ONe novae), more massive than CO ones, provide large enrichments not only in CNO nuclei, but also in neon, sodium, aluminum, or other intermediate-mass elements (Starrfield et al. 1998; José & Hernanz 1998; José et al. 1999). Hence, the composition of the ejecta is a key signature of the nature of the underlying white dwarf (CO or ONe) and provides also valuable information on the explosion (i.e., peak temperature, characteristic timescale...). In particular, the presence of isotopes of the silicon to calcium mass region (hereafter, Si-Ca), overproduced with respect to solar values, in the ejecta of a classical nova, may reveal the presence of an underlying massive white dwarf (the ones reaching the higher peak temperatures during the explosion) since proton captures on nuclei above silicon require temperatures in excess of 3×10^8 K to overcome their large Coulomb barriers. Indeed, abundance determinations from some observed novae, such as V1370 Aql 1982 (Snijders et al. 1987), QU Vul 1984 (Andreä et al. 1994), V2214 Oph 1988 (Andreä et al. 1994), or V838 Her 1991 (Vanlandingham et al. 1996, 1997), show the presence of Si-Ca nuclei in the ejecta.

Moreover, the nova contribution to the Galactic content of other species such as ^7Li (Starrfield et al. 1978, Hernanz et al. 1996) or ^{26}Al (Politano et al. 1995, José et al. 1997, Starrfield et al. 1998, José et al. 1999) may also be significant, although its real extent is still a matter of debate (see Romano et al. 1999, for details on the contribution of novae to match the ^7Li content in realistic calculations of Galactic Chemical evolution). The synthesis of such medium- or long-lived species has, in turn, implications for the high-energy emission during nova outbursts: several gamma-ray signatures have been predicted for nova outbursts (Clayton & Hoyle 1974; Leising & Clayton 1987; Gómez-Gomar et al. 1998, Hernanz et al. 1999), including a 478 keV line from ^7Li (CO novae), a 1275 keV line from ^{22}Na (ONe novae), and an intense 511 keV line and the corresponding continuum at energies below (for both CO and ONe nova types). In the Si-Ca mass region, another gamma-ray signal, coming from the β^+ -decay of the medium lived ^{34m}Cl (isomeric state), has also been proposed for 511 keV (Leising & Clayton 1987) and 2.128 MeV (Coc et al. 2000a) line emission. However, no nucleosynthesis calculation with realistic nuclear reaction rates has, up to now, been attempted to evaluate the chances for the potential detection of this particular gamma-ray

signal from novae.

Furthermore, the recent discovery of a number of presolar grains likely formed in the ejecta of classical novae (Amari et al., 2001) also points out the importance of a good determination of the abundance pattern, in particular in the Si-Ca mass region: together with a number of constraints from specific isotopic ratios (i.e., low $^{12}\text{C}/^{13}\text{C}$ and $^{14}\text{N}/^{15}\text{N}$ values, high $^{26}\text{Al}/^{27}\text{Al}$), the basic feature that points towards a nova origin relies on the large excesses in $^{30}\text{Si}/^{28}\text{Si}$ and close-to-solar $^{29}\text{Si}/^{28}\text{Si}$ measured in such grains. The determination of other isotopic ratios in this mass range, such as $^{33}\text{S}/^{32}\text{S}$, may also help to identify future nova grain candidates.

These aspects point out the interest of a more accurate determination of the relevant synthesis mechanisms in the Si-Ca mass region. Such an analysis has been only scarcely attempted (see recent parametrized nucleosynthesis calculations by Lefevbre et al. 1997, Wanajo et al. 1999, and Iliadis et al. 1999, as well as hydrodynamic calculations by Starrfield et al. 1998), partially because of the large number of isotopes of interest in this mass region, around 40 species, and the hundred nuclear reactions involved. Accordingly, it is the purpose of this paper to determine the dominant nuclear paths involved in the synthesis of intermediate-mass elements, from Si to Ca, during classical nova outbursts, identifying the key reactions and investigating their associated nuclear uncertainties, that may have a dramatic influence in the overall process. In Section 2, we outline the basic nuclear paths at different stages of the nova outburst for a particular model. Details on nuclear physics aspects are given in Section 3. Constraints on the production of Si-Ca group nuclei, together with the most relevant conclusions of this paper are summarized in Section 4.

2. Main nuclear paths in the synthesis of Si-Ca nuclei in classical novae

The high temperatures required to initiate a noticeable nuclear activity in the Si-Ca group nuclei restrict the domain of interest to explosions in very massive white dwarfs (i.e., close to the Chandrasekhar mass). In this section, we will focus on the main nuclear paths involved in the synthesis of several isotopes within this mass range, through a detailed analysis of a $1.35 M_{\odot}$ ONe white dwarf, which accretes solar-like matter at a rate of $\dot{M} = 2 \times 10^{-10} M_{\odot} \cdot \text{yr}^{-1}$, assuming a 50% degree of mixing with the outermost shells of the white dwarf core. Initial abundances of the Si-Ca group nuclei adopted in this Model are listed in Table 1 (abundances up to Si are given in José et al. 1999, Table 1). In fact, the specific prescription adopted for the initial abundance pattern is crucial for nucleosynthesis calculations. Whereas a deep analysis of this effect is out of the scope of this paper, and will be presented elsewhere, we just point out that it introduces some uncertainty in all current

nucleosynthesis calculations during nova outbursts.

The main source for the production of the Si–Ca isotopes (see Fig. 1) comes from the processing of the initial Ne–Al isotopes from the white dwarf leaking out of the NeNa and MgAl mass regions, mainly through ^{28}Si . We do not discuss here the nuclear processing within these regions but refer the reader to a previous paper (José et al. 1999). Hence we start our discussion with the last reactions linking the MgAl to SiP mass regions. The new evolutionary sequences of nova outbursts have been calculated by means of the code SHIVA (see José & Hernanz 1998 for details), a one-dimensional implicit hydrodynamical code that follows the course of the explosion from the onset of accretion up to the ejection stages. Calculations have been performed with a nuclear reaction network updated for the region of interest (see section 3). Snapshots of the evolution of the most relevant elements are shown in Figures 2 to 6.

At the early stages of the explosion, nuclear activity above CNO cycle is mostly confined in the NeNa and MgAl region with only marginal activity in the Si–Ca region. Soon after the thermonuclear runaway takes place, when the temperature at the burning shell reaches $T_{bs} = 8 \times 10^7$ K (Figs. 2 to 6, first panel), the main nuclear path affecting Si to Ca evolution is dominated by a series of reactions, beginning with proton captures onto ^{26g}Al (ground state), $^{26g}\text{Al}(p,\gamma)^{27}\text{Si}$, followed by $^{27}\text{Si}(\beta^+)^{27}\text{Al}(p,\gamma)^{28}\text{Si}$. As a result, ^{27}Si is slightly enhanced at the burning shell, since its β^+ -decay channel is slower than $^{26g}\text{Al}(p,\gamma)$. Marginal nuclear activity at the burning shell involves other proton-capture reactions on ^{25}Al and ^{26m}Al (isomeric state), as well as onto ^{27}Si , which account for a moderate increase in ^{26}Si and ^{28}P . No relevant nuclear activity beyond phosphorus is found.

Evolution at $T_{bs} = 10^8$ K (Figs. 2 to 6, second panel) is still dominated by the chain $^{26g}\text{Al}(p,\gamma)^{27}\text{Si}(\beta^+)^{27}\text{Al}(p,\gamma)^{28}\text{Si}$, plus the contribution of $^{25}\text{Al}(p,\gamma)^{26}\text{Si}(\beta^+)^{26m}\text{Al}(p,\gamma)^{27}\text{Si}$, and $^{27}\text{Si}(p,\gamma)^{28}\text{P}(\beta^+)^{28}\text{Si}$. Some marginal activity involves also $^{31}\text{P}(p,\gamma)^{32}\text{S}$, and $^{34}\text{S}(p,\gamma)^{35}\text{Cl}$. The most remarkable feature at this stage is an important increase in both $^{26,27}\text{Si}$. The outermost shells are dominated by some marginal decays (the lower temperatures prevent proton captures to proceed efficiently), such as $^{27}\text{Si}(\beta^+)^{27}\text{Al}$, $^{26}\text{Si}(\beta^+)^{26m}\text{Al}$, and $^{30}\text{P}(\beta^+)^{30}\text{Si}$, followed by $^{29}\text{P}(\beta^+)^{29}\text{Si}$, and $^{34m}\text{Cl}(\beta^+)^{34}\text{S}$.

Important changes take place as soon as T_{bs} reaches 2×10^8 K (Figs. 2 to 6, third panel). The nuclear activity is now driven by $^{26g}\text{Al}(p,\gamma)^{27}\text{Si}(p,\gamma)^{28}\text{P}$ (faster than $^{27}\text{Si}(\beta^+)^{27}\text{Al}$), and by $^{27}\text{Al}(p,\gamma)^{28}\text{Si}$, followed by $^{25}\text{Al}(p,\gamma)^{26}\text{Si}(\beta^+)^{26m}\text{Al}(p,\gamma)^{27}\text{Si}(\beta^+)^{27}\text{Al}$, $^{28}\text{P}(\beta^+)^{28}\text{Si}$, $^{26}\text{Si}(p,\gamma)^{27}\text{P}(\beta^+)^{27}\text{Si}$, $^{28}\text{P}(p,\gamma)^{29}\text{S}$, and $^{28,29}\text{Si}(p,\gamma)^{29,30}\text{P}$. The outermost shells are dominated by $^{27}\text{Si}(\beta^+)^{27}\text{Al}$, $^{26}\text{Si}(\beta^+)^{26m}\text{Al}$, and $^{28}\text{P}(\beta^+)^{28}\text{Si}$, followed by $^{27,29,30}\text{P}(\beta^+)^{27,29,30}\text{Si}$. One of the most relevant outcomes is a substantial increase in both $^{26,27}\text{Si}$ which, except for ^{28}Si , become the most abundant silicon isotopes in the envelope now. In fact ^{27}Si attains its max-

imum value at this stage (soon after, as the temperature rises towards T_{peak} , it begins to be destroyed by proton captures). Concerning ^{28}Si , it has significantly increased in the burning shell, up to 2.5×10^{-3} , by mass. On the contrary, ^{29}Si has been slightly destroyed at the burning shell by (p,γ) reactions, whereas ^{30}Si remains mostly unaffected. Major activity involves also several phosphorus isotopes: whereas ^{31}P remains close to its initial abundance, major synthesis of ^{28}P (reaching 4.4×10^{-4} by mass, at the burning shell) and $^{27,29,30}\text{P}$ ($\sim 10^{-6}$, by mass) is also reported. Only one sulfur isotope, ^{29}S , shows a noticeable variation: it is, in fact, increased by (p,γ) reactions on ^{28}P nuclei at the burning shell, and shortly after, carried away to the outer envelope by means of convective transport. No significant nuclear path involving Cl, Ar, K or Ca is found yet.

When T_{bs} reaches 3×10^8 K (Figs. 2 to 6, fourth panel), the major nuclear activity is dominated by $^{28}\text{Si}(p,\gamma)^{29}\text{P}(p,\gamma)^{30}\text{S}$, $^{27}\text{Si}(p,\gamma)^{28}\text{P}(\beta^+)^{28}\text{Si}$, $^{25}\text{Al}(p,\gamma)^{26}\text{Si}(p,\gamma)^{27}\text{P}(\beta^+)^{27}\text{Si}$, $^{26m}\text{Al}(p,\gamma)^{27}\text{Si}$ plus $^{30}\text{P}(p,\gamma)^{31}\text{S}$. One of the most relevant outcomes related to the synthesis of S to Ca isotopes is the key role played by ^{30}P in the evolution: in fact, $^{30}\text{P}(p,\gamma)^{31}\text{S}$ controls the path towards heavier species, partially because the path through ^{29}P (i.e., $^{29}\text{P}(p,\gamma)^{30}\text{S}(p,\gamma)^{31}\text{Cl}$) is inhibited by the efficient inverse photodisintegration reaction $^{31}\text{Cl}(\gamma, p)^{30}\text{S}$, which is rapidly followed by a β^+ -decay, leading to ^{30}P . Hence ^{30}P is a mandatory passing point to ^{32}S via $^{30}\text{P}(p,\gamma)^{31}\text{S}(p,\gamma)^{32}\text{Cl}(\beta^+)^{32}\text{S}$ or through $^{30}\text{P}(p,\gamma)^{31}\text{S}(\beta^+)^{31}\text{P}(p,\gamma)^{32}\text{S}$, while $^{30}\text{P}(\beta^+)^{30}\text{Si}(p,\gamma)^{31}\text{P}(p,\gamma)^{32}\text{S}$ is strongly inhibited by the slow ^{30}P β^+ -decay.

Other important reactions at this stage include $^{24,26g,27}\text{Al}(p,\gamma)^{25,27,28}\text{Si}$, $^{26}\text{Si}(\beta^+)^{26m}\text{Al}$, $^{28}\text{P}(p,\gamma)^{29}\text{S}(\beta^+)^{29}\text{P}(\beta^+)^{29}\text{Si}(p,\gamma)^{30}\text{P}$ and $^{30,31}\text{S}(\beta^+)^{30,31}\text{P}$. A minor role is also played by $^{25}\text{Si}(\beta^+)^{25}\text{Al}$, $^{30}\text{P}(\beta^+)^{30}\text{Si}$, $^{30}\text{S}(p,\gamma)^{31}\text{Cl}$ and its reverse reaction $^{31}\text{Cl}(\gamma,p)^{30}\text{S}$, and both (p,γ) and (p,α) reactions on ^{31}P . The outermost envelope, much cooler, is dominated by β^+ -decays from $^{26,27}\text{Si}$, $^{29,30}\text{P}$ and marginally from ^{28}P and ^{37}K . The number of nuclei involved in the different dominant paths is, at this stage, very large: the most abundant silicon isotope, ^{28}Si , has already reached 3.3×10^{-2} in the inner envelope. ^{26}Si attains now its maximum value in the envelope. Regarding ^{27}Si , it shows a peculiar profile, with a 'hump' at intermediate shells. This reflects the fact that, whereas it is destroyed at the burning shell (where (p,γ) reactions dominate synthesis from $^{27}\text{P}(\beta^+)$) and at the outer part of the envelope (through β^+ -decays), it is enhanced by $^{26g}\text{Al}(p,\gamma)$ at such intermediate shells. A similar trend is found for ^{29}Si : destroyed by (p,γ) reactions in the inner envelope, and synthesized by $^{29}\text{P}(\beta^+)$ at intermediate shells. ^{30}Si increases only by a small amount.

Concerning phosphorus, all isotopes are enhanced at this stage: $^{27,28,30}\text{P}$ reach $\sim 10^{-3}$, by mass, whereas ^{29}P , the most abundant phosphorus isotope so far, achieves $\sim 10^{-2}$. ^{31}P reaches $\sim 10^{-4}$ at the burning shell. Except for ^{37}Cl (slightly destroyed at the burning shell), all other chlorine isotopes are enhanced. The most abundant one, ^{35}Cl , reaches a mass-

fraction of 5.6×10^{-6} . The profile of ^{31}Cl shows also a hump at intermediate shells, which distinguishes the region where destruction by $^{31}\text{Cl}(p,\gamma)$ dominates synthesis by $^{30}\text{S}(p,\gamma)^{31}\text{Cl}$ (innermost envelope) from that where synthesis by $^{30}\text{S}(p,\gamma)^{31}\text{Cl}$ dominates destruction by both proton captures and β^+ -decays (the evolution of ^{31}Cl in the outermost envelope is dominated by $^{31}\text{Cl}(\beta^+)$).

Evolution of sulfur isotopes mainly affects $^{29-31}\text{S}$, which show a dramatic increase powered by (p,γ) reactions on $^{28-30}\text{P}$. In fact, ^{30}S becomes the most abundant sulfur isotope at this stage. Moderate enhancement of ^{32}S and destruction of $^{33,34,36}\text{S}$ is also reported. Some marginal activity involves also Ar and K, mainly affecting $^{34,35,37}\text{Ar}$, enhanced at the burning shell, and ^{38}Ar , which moderately decreases.

The course of the thermonuclear runaway drives the burning shell up to a peak temperature of $T_{max} = 3.26 \times 10^8$ K (Figs. 2 to 6, panel fifth). The main nuclear activity is now driven by $^{25}\text{Al}(p,\gamma)^{26}\text{Si}(p,\gamma)^{27}\text{P}$ and the chain $^{27}\text{Si}(p,\gamma)^{28}\text{P}(\beta^+)^{28}\text{Si}(p,\gamma)^{29}\text{P}(p,\gamma)^{30}\text{S}(\beta^+)^{30}\text{P}(p,\gamma)^{31}\text{S}(\beta^+)^{31}\text{P}(p,\gamma)^{32}\text{S}$. Significant activity also involves $^{24}\text{Al}(p,\gamma)^{25}\text{Si}(\beta^+)^{25}\text{Al}$, $^{26}\text{Si}(\beta^+)^{26m}\text{Al}(p,\gamma)^{27}\text{Si}$, $^{26g}\text{Al}(p,\gamma)^{27}\text{Si}$, $^{27}\text{P}(\beta^+)^{27}\text{Si}$, $^{28}\text{P}(p,\gamma)^{29}\text{S}(\beta^+)^{29}\text{P}(\beta^+)^{29}\text{Si}(p,\gamma)^{30}\text{P}$, $^{31}\text{P}(p,\alpha)^{28}\text{Si}$ and $^{30}\text{S}(p,\gamma)^{31}\text{Cl}$ and its reverse photodisintegration reaction. At this stage, protons are energetic enough to overcome the Coulomb potential barrier of many nuclei, in particular ^{28}Si which, for the first time, begins to decrease at the burning shell. Reduction of $^{26,27}\text{Si}$ and a noticeable enhancement of $^{29,30}\text{Si}$ is also found. Concerning phosphorus, $^{29,30}\text{P}$ but mainly ^{31}P increase at this stage. β^+ -decays are responsible for a significant reduction of both $^{27,28}\text{P}$. The most relevant feature regarding the evolution of sulfur isotopes is an important increase of $^{30-33}\text{S}$. In fact, at this stage, ^{31}S becomes the most abundant sulfur isotope in the envelope. ^{33}Cl is favored also by the rise in temperature, and becomes now the most abundant chlorine isotope in the vicinity of the burning shell. $^{32,34g,34m}\text{Cl}$ are also enhanced during this stage. Nuclear activity affects now the edge of the network, with some enhancement of heavier species, such as $^{34,35,37}\text{Ar}$, $^{37,38}\text{K}$ and, to some extent, ^{39}Ca . However, the moderately low nuclear reaction fluxes in this region justifies our choice of ^{40}Ca as the last isotope of the network. As earlier in the evolution of the nova outburst, the outer envelope is again dominated by β^+ -decays such as $^{26,27}\text{Si}(\beta^+)^{26m,27}\text{Al}$ and $^{29,30}\text{P}(\beta^+)^{29,30}\text{Si}$.

Due to the sudden release of energy from the short-lived β^+ -unstable nuclei ^{13}N , $^{14,15}\text{O}$ and ^{17}F , the envelope begins to expand. A hundred seconds after T_{peak} , the envelope reaches a size of 10^9 cm (Figs. 2 to 6, sixth panel). At this stage, the burning shell is dominated by $^{26g}\text{Al}(p,\gamma)^{27}\text{Si}(p,\gamma)^{28}\text{P}(\beta^+)^{28}\text{Si}(p,\gamma)^{29}\text{P}$, $^{29}\text{Si}(p,\gamma)^{30}\text{P}(p,\gamma)^{31}\text{S}$, and $^{31}\text{P}(p,\gamma)^{32}\text{S}$, plus a significant contribution from $^{25}\text{Al}(p,\gamma)^{26}\text{Si}(\beta^+)^{26m}\text{Al}(p,\gamma)^{27}\text{Si}$, $^{27}\text{Si}(\beta^+)^{27}\text{Al}(p,\gamma)^{28}\text{Si}$, $^{29}\text{P}(\beta^+)^{29}\text{Si}$, $^{29}\text{P}(p,\gamma)^{30}\text{S}(\beta^+)^{30}\text{P}(\beta^+)^{30}\text{Si}(p,\gamma)^{31}\text{P}(p,\alpha)^{28}\text{Si}$, $^{31}\text{S}(\beta^+)^{31}\text{P}$, and $^{32,34}\text{S}(p,\gamma)^{33,35}\text{Cl}$. The expansion of the envelope, which is accompanied by a drop in temperature, provides a quite

different chemical pattern above the burning shell. In particular, the evolution of the Si-Ca nuclei is fully dominated by β^+ -decays (the most important ones being $^{28-30}\text{P}(\beta^+)^{28-30}\text{Si}$, $^{27}\text{Si}(\beta^+)^{27}\text{Al}$, and $^{31}\text{S}(\beta^+)^{31}\text{P}$, at the inner shells, whereas the outer envelope is dominated by $^{29,30}\text{P}(\beta^+)^{29,30}\text{Si}$, $^{34m}\text{Cl}(\beta^+)^{34}\text{S}$, and $^{38}\text{K}(\beta^+)^{38}\text{Ar}$). At this stage of the evolution, the envelope shows dramatic changes in composition. In particular, isotopes such as $^{28,29,30}\text{Si}$, $^{30,31}\text{P}$, $^{32-34}\text{S}$, ^{35}Cl , $^{36,37}\text{Ar}$ or ^{38}K show a significant enhancement whereas ^{26}Si , $^{29-31}\text{S}$, $^{27-29}\text{P}$, $^{31-34}\text{Cl}$, or ^{34}Ar are efficiently destroyed.

During the final stages of the outburst (Figs. 2 to 6, seventh panel), convection recedes from the surface and the burning shell becomes detached from the major part of the envelope, which is ultimately ejected. When the envelope reaches a size of 10^{10} cm, the main nuclear path in the Si-Ca region is basically carried by $^{28-30}\text{P}(\beta^+)^{28-30}\text{Si}$, $^{26,27}\text{Si}(\beta^+)^{26m,27}\text{Al}$, $^{30,31}\text{S}(\beta^+)^{30,31}\text{P}$, and $^{33}\text{Cl}(\beta^+)^{33}\text{S}$, with $^{30}\text{P}(\beta^+)^{30}\text{Si}$ being the dominant one within most of the envelope (again, contribution from $^{34m}\text{Cl}(\beta^+)^{34}\text{S}$ and $^{38}\text{K}(\beta^+)^{38}\text{Ar}$ are important in the outer envelope).

Soon after, when the envelope reaches a size of 10^{12} cm (Figs. 2 to 6, eighth panel), most of the β^+ -unstable nuclei have already decayed. Only the medium-lived ones ($\tau \sim$ minutes), contribute yet to the energy production: $^{30}\text{P}(\beta^+)^{30}\text{Si}$, $^{34m}\text{Cl}(\beta^+)^{34}\text{S}$, and $^{38}\text{K}(\beta^+)^{38}\text{Ar}$. The mean composition of the ejecta in the Si-Ca mass region consists, for this particular model, mainly of $^{28-30}\text{Si}$, ^{32}S , and ^{31}P . The most overproduced species with respect to solar are ^{31}P and ^{30}Si , with overproduction factors (i.e., ratios between mean mass fractions in the ejecta over solar values) 1100 and 600, respectively. $^{32,33}\text{S}$ are overproduced by a factor ~ 100 .

In summary, nuclear activity in the Si–Ca mass region is powered by leakage from the NeNa–MgAl region, where the activity is confined during the early stages of the outburst. The main nuclear reaction that drives nuclear activity towards heavier species beyond sulfur is $^{30}\text{P}(\text{p},\gamma)$, through two different paths: either $^{30}\text{P}(\text{p},\gamma)^{31}\text{S}(\text{p},\gamma)^{32}\text{Cl}(\beta^+)^{32}\text{S}$ or $^{30}\text{P}(\text{p},\gamma)^{31}\text{S}(\beta^+)^{31}\text{P}(\text{p},\gamma)^{32}\text{S}$. Then, the nuclear flow is dramatically reduced by the slow $^{32}\text{S}(\text{p},\gamma)$ limiting the production of heavier isotopes in the S–Ca mass range.

3. Nuclear reaction rates in the Si-Ca mass region

3.1. Proton captures on silicon isotopes

The rates of the $^{26,27}\text{Si}(\text{p},\gamma)$ reactions have been discussed in José et al. (1999). These reactions do not play a dominant role in the path towards heavier species as photodisintegration of ^{27}P is effective (low Q-value) and because the $^{27,28}\text{P}$ lifetimes are small (< 1 s). The $^{28}\text{Si}(\text{p},\gamma)^{29}\text{P}$ reaction is the only significant leak from the Ne–Al region towards heavier

nuclei (Figure 1). Hence it is natural to begin our analysis at this point, referring for the discussion of rates in the Ne–Al chains to our previous paper (José et al. 1999). Except for the very recent work of Iliadis et al. (2001), published after this work was completed, the two last compilations of thermonuclear rates end at silicon, either with $^{30}\text{Si}(p,\gamma)^{31}\text{P}$ (Caughlan & Fowler 1988, hereafter CF88) or $^{28}\text{Si}(p,\gamma)^{29}\text{P}$ (Angulo et al. 1999, hereafter NACRE). The $^{28}\text{Si}(p,\gamma)^{29}\text{P}$ rate from NACRE differs significantly from the CF88 one but only below 10^8 K, while the $^{29,30}\text{Si}(p,\gamma)$ reaction rates should not deviate much from the CF88 ones at nova temperatures (Angulo, 2000). Accordingly, in this paper we have used the $^{28-30}\text{Si}(p,\gamma)$ rates from CF88.

3.2. Proton captures on phosphorus isotopes

The $^{29}\text{P}(p,\gamma)^{30}\text{S}$ rate was calculated by Wiescher & Görres (1988) from the properties of the T=1 isospin triplet. The positions of the first levels above threshold in ^{30}S were calculated by the Thomas–Ehrman shift method while the spectroscopic factors were taken from the analog levels in ^{30}Si . This rate is for the moment rather poorly known at nova temperatures as a consequence, in particular, of the uncertainty on the calculated position of the first resonance. However, this reaction rate is not crucial as there exists an alternative link to heavier isotopes initiated by the ^{29}P β^+ -decay (Figure 1). For the $^{30}\text{P}(p,\gamma)^{31}\text{S}$ rate (6.0371D+01, 8.6903D-01,-5.3250D+01, -4.5676D+00, 1.7458D+00,-1.5449D-01,-1.1437D+01, in REACLIB format), we use the result of a statistical model calculation (Thielemann et al. 1987, hereafter SMOKER), because of the lack of spectroscopic information on ^{31}S . Indeed, even though 17 levels are known up to 1 MeV above threshold, very few spins are reported. Hence, it is not possible to calculate a realistic reaction rate based neither on ^{31}P analog levels nor shell model calculations (Endt 1998). However, the statistical model assumes a high level density which is *a priori* favored by the high Q-value (6.133 MeV) but remains questionable at the moderate temperatures found in novae. Hence, with such a level density, it is more likely that the rate is governed by the properties of a few individual levels.

The inspection of Figure 1, shows that this reaction plays a key role as ^{30}P is a mandatory passing point to reach heavier nuclei and with its relatively long lifetime ($t_{1/2}=2.5$ mn) it stops further nucleosynthesis unless proton captures are fast enough. Accordingly we investigate the effect of a possible change of this rate by a test factor of 100 (see Section 4). The $^{31}\text{P}(p,\gamma)^{32}\text{S}$ and $^{31}\text{P}(p,\alpha)^{28}\text{Si}$ reaction rates are deduced from experimental results (Iliadis et al. 1991; 1993; Ross et al. 1995). While the first one is well known, the second still suffers from uncertainties ($\lesssim 100$) between $T_9 = 0.1$ and 0.2 due to unknown resonance strengths.

However, even the upper limit of the $^{31}\text{P}(p,\alpha)^{28}\text{Si}$ rate remains smaller than the $^{31}\text{P}(p,\gamma)^{32}\text{S}$ one at nova temperature. Hence this uncertainty should scarcely affect ^{31}P destruction and nucleosynthesis beyond phosphorus.

3.3. Proton captures on sulfur isotopes and beyond

For $^{30}\text{S}(p,\gamma)^{31}\text{Cl}$, we use the rate calculated by Herndl et al. (1995) from shell model calculations. Another rate was provided by Van Wormer et al. (1994) based on the properties of the analog levels in ^{31}Cl . The two rates differ by a factor of $\lesssim 30$ (Fig. 1 in Herndl et al. (1995)) due to the unknown location of the first excited state in ^{31}Cl . This should however have little effect since photodisintegration of ^{31}Cl is fast ($Q=0.286$ MeV). The $^{31}\text{S}(p,\gamma)^{32}\text{Cl}$ reaction rate was first studied by Vouzoukas et al. (1994). They measured the energy of the relevant ^{32}Cl levels via a $^{32}\text{S}(^3\text{He},t)^{32}\text{Cl}$ transfer reaction. They used experimental spectroscopic factors from the ^{32}P analog levels and radiative widths from shell model calculations and their calculated ratios (Γ_γ/Γ_T) are compatible with the Lefevbre et al. (1997) measurements. A detailed investigation of the uncertainty affecting this rate has been performed recently by Iliadis et al. (1999) leading to a nominal rate (adopted here) slightly lower than the previous one (Vouzoukas et al. 1994), and a factor of 3 uncertainty in the domain of nova nucleosynthesis. One can thus consider this rate as sufficiently known. The $^{32}\text{S}(p,\gamma)^{33}\text{Cl}$ reaction rate was calculated by Iliadis et al. (1992) from measured resonance strengths or extracted spectroscopic factors (see also Iliadis et al. 1999, footnote in Table 7). The uncertainty on this rate was found to be very small (Thompson & Iliadis 1999). It is important to notice that the rate deduced from experimental data is much smaller (see Iliadis et al. 1992) than the previously adopted reaction rate.

For the reactions $^{33}\text{S}(p,\gamma)^{34g,34m}\text{Cl}$, we have taken into account the formation of both the ^{34}Cl ground ($t_{1/2} = 1.53$ s) and isomeric ($t_{1/2} = 32.0$ min) states which, as in ^{26}Al , have to be treated as separate isotopes (Coc et al. 2000a) at nova temperatures. We considered the resonances corresponding to the first five levels above threshold (Endt 1990). Their branching ratios to the ground or isomeric states were extracted from Endt (1990). For the four unknown resonance strengths, we used upper limits with the usual 0.1 reduction factor. They were obtained from estimates of the proton widths ($\Gamma_p \ll \Gamma_\gamma$) based on calculation of single particle in a Wood-Saxon potential whose depth is adjusted so as to reproduce the excitation energy of the resonance. The corresponding estimated $^{33}\text{S}(p,\gamma)^{34m}\text{Cl}$ rate is given by:

$$N_A \langle \sigma v \rangle = \begin{aligned} & 1.5923 \times 10^5 T_9^{-3/2} \times (0 \text{ to } 1) \times \\ & (2.4 \times 10^{-29} \exp(-0.3389/T_9) \times 1. \end{aligned}$$

$$\begin{aligned}
 &+1.5 \times 10^{-13} \exp(-2.003/T_9) \times 0.89 \\
 &+2.4 \times 10^{-5} \exp(-2.836/T_9) \times 0.64 \\
 &+1. \times 10^{-3} \exp(-4.623/T_9) \times 0.76) \\
 &+2.13 \times 10^4 T_9^{-0.1493} \exp(-4.814/T_9) \times 0.5
 \end{aligned}$$

where the multiplying factors (1., 0.89, 0.64, 0.76 and 0.5) correspond to the branching ratios to the isomeric state (Endt 1990). The $^{33}\text{S}(p,\gamma)^{34g}\text{Cl}$ is hence given by replacing these factors by (0., 0.11, 0.36, 0.24 and 0.5). The last term is a multiresonant contribution from the higher energy resonances (Endt 1990) with an assumed average branching ratio of 0.5.

Formation of ^{34m}Cl proceeds only through the $^{33}\text{S}(p,\gamma)^{34m}\text{Cl}$ reaction since, after internal transitions, ^{34}Ar β^+ -decays lead only to ^{34g}Cl (a similar configuration is found for ^{26}Al). An important aspect of ^{34m}Cl nucleosynthesis is its destruction by thermally induced radiative transitions to its short lived ground state. The corresponding effective lifetime, that we use here, has been calculated (Shell Model) by Coc et al. (2000a): it exhibits a rapid evolution (3 orders of magnitude) from its laboratory half-life value of 32.0 min down to ≈ 1 s. This transition occurs around $T_9 \approx 0.15$ -0.2, a typical domain of temperatures in novae, and this strongly modifies the prospect for its detectability through its gamma-ray signature. Other nuclei, such as ^{24}Al , have also isomers in the mass region of nova nucleosynthesis but they are at the fringe of nuclear flow and their lifetimes are much less affected than ^{34}Cl at nova temperatures.

With some notable exceptions like $^{35}\text{Cl}(p,\gamma)$ and $^{36}\text{Ar}(p,\gamma)$ (see also the very recent compilation of Iliadis et al. 2001), experimental and theoretical (i.e., Shell Model, see Herndl et al. 1995) data are in general not sufficient to allow the explicit calculation of the rates at nova temperatures for reactions beyond sulfur. Accordingly, we use the SMOKER rates instead (Thielemann et al. 1987) which are virtually identical to the more recent MOST rates from Goriely (1996), for these nuclei close to stability.

4. Results and discussion

Table 2 shows the mean composition of the ejecta, for the Si-Ca mass region, corresponding to the $1.35 M_{\odot}$ ONe nova described in Section 2 (hereafter, Model 135nom). The most abundant nuclei, for this specific mass range, are ^{32}S , ^{28}Si , ^{30}Si , ^{31}P and ^{29}Si . For the purpose of comparison, a very similar model (i.e., Model ONe135B. See José, Coc & Hernanz 1999), computed with a previous nuclear reaction network, is also shown in Table 2. Both nuclear reaction networks are very similar up to silicon. Recent updates included in the new com-

putations involve $^{18}\text{F}(\text{p},\gamma)$, $^{18}\text{F}(\text{p},\alpha)$ (Coc et al. 2000b, nominal rates), $^{17}\text{O}(\text{p},\gamma)$, $^{17}\text{O}(\text{p},\alpha)$ (NACRE, nominal rates), and also $^{31}\text{P}(\text{p},\gamma)$, $^{31}\text{P}(\text{p},\alpha)$, $^{31}\text{S}(\text{p},\gamma)$, $^{32}\text{S}(\text{p},\gamma)$, $^{33}\text{S}(\text{p},\gamma)$ (leading to both $^{34g,34m}\text{Cl}$), and the corresponding $^{34g,34m}\text{Cl}$, temperature-dependent β^+ -decays (see Section 3 for specific references). As expected, no significant differences are found for Si or P yields when we switch to the updated network since, as discussed in Coc et al. (2000b), proton captures onto ^{17}O or ^{18}F don't play a dominant role in the energetics of the explosion, and hence, a similar peak temperature and characteristic timescales for the evolution are found. Differences, however, are found for ^{32}S and beyond. In fact, the new ^{32}S yield increases by a factor of 2, because of the larger new $^{31}\text{P}(\text{p},\gamma)$ rate (below 10^8 K and also in the vicinity of T_{peak}) and the lower $^{32}\text{S}(\text{p},\gamma)^{33}\text{Cl}$ destruction rate. On the contrary, $^{33,34}\text{S}$, $^{35,37}\text{Cl}$ and $^{36,38}\text{Ar}$ are dramatically reduced by, at least, a factor of 10. This remarkable change results mainly from the update of the $^{32}\text{S}(\text{p},\gamma)$ rate, much lower than the previous one in the domain of nova temperatures, as pointed out by Iliadis et al. (1992). Hence, whereas the arguments to invoke a likely nova origin for a number of presolar meteoritic grains (see Amari et al. 2001) remain unaffected by the results reported in this paper (i.e., silicon excesses), the differences found for other nuclear species, in particular the $^{32}\text{S}/^{33}\text{S}$ ratios, are relevant for the unambiguous identification of future nova grain candidates: for instance, the previous $^{32}\text{S}/^{33}\text{S}$ isotopic ratio of 3.1, found for Model ONe135B, has now raised up to 97 for Model 135nom, basically due to the update of the $^{31}\text{P}(\text{p},\gamma)$ and $^{32}\text{S}(\text{p},\gamma)$ rates.

It is also worth noting that our numerical calculations reveal the presence of the gamma-ray emitter ^{34m}Cl in the ejected envelope. However, its content has been dramatically reduced by the update of the $^{32}\text{S}(\text{p},\gamma)^{33}\text{Cl}$ and $^{33}\text{S}(\text{p},\gamma)^{34m,34g}\text{Cl}$ rates, together with the ^{34m}Cl β^+ -decay: whereas a mean mass fraction of 3.4×10^{-3} , 30 minutes after T_{peak} , was found for Model ONe135B, only 7×10^{-7} by mass, remain, for the same time, in the present Model 135nom. Hence, the possibility of a potential detection of the gamma ray emission corresponding to ^{34m}Cl β^+ -decay, invoked as another signature of a classical novae (see Leising & Clayton 1987), seems to be ruled out with the present calculations.

As pointed out, one of the most relevant outcomes of this study, from the nuclear physics viewpoint, is the crucial role played by $^{30}\text{P}(\text{p},\gamma)$ in the synthesis of heavier nuclear species. Its purely theoretical rate is questionable since the model used for its calculation reaches its limits for such a light nucleus at low temperature. Hence, we have estimated its impact on the yields by computing two new evolutionary sequences of nova models, for which we have arbitrarily modified the $^{30}\text{P}(\text{p},\gamma)$ rate: Model p30low, where the $^{30}\text{P}(\text{p},\gamma)$ has been reduced by a test factor of 100 throughout the calculation, and Model p30high, where the nominal rate has been arbitrarily multiplied by 100. Results are summarized also in Table 2. The increase by a factor of 100 affects only the ^{30}Si yield: since the path towards ^{31}S is favored (which in turn, accounts for the moderate increase of ^{31}P in the ejecta), much less

^{30}Si (coming from $^{30}\text{P}(\beta^+)$) is left in the envelope. However, the impact on other nuclear species is very limited. On the contrary, when the $^{30}\text{P}(\text{p},\gamma)$ rate is reduced by a factor of 100, dramatic changes in the expected yields occur. Now, $^{30}\text{P}(\beta^+)$ competes favorably with proton captures, and an important enhancement of ^{30}Si is obtained. In fact, the reduction of the proton capture rate halts significantly the synthesis of elements above Si (by a factor of ~ 10 with respect to the values found with the nominal rate). We have compared our results with the latest available results from hydrodynamic simulations of ONe novae by Starrfield et al. (2001): they state that the switch to an updated nuclear network (Iliadis et al. 2001) is accompanied by an important reduction of the abundances of nuclei above aluminum, in good agreement with the results found here. However, our new computations show that reduction of the yields affect only nuclei above ^{32}S . In fact, a significant reduction of ^{32}S results only when we adopt the low $^{30}\text{P}(\text{p},\gamma)$ test rate. Hence, this discrepancy might be likely attributed to a different prescription for the adopted $^{30}\text{P}(\text{p},\gamma)$ rate. In particular, the rate used by Starrfield et al. (2001) seems to be somewhat lower than the nominal rate adopted in our paper, which stresses again the crucial dependence of the S–Ca yields on this particular rate.

Despite a detailed comparison with observations is out of the scope of this paper, because a larger number of nova models is required to properly explore the wide parameter space, some conclusions can be outlined. In fact, spectroscopic abundance determinations show evidence for some overproduction of nuclei in the Si–Ca mass region in a number of classical novae, including silicon (Nova Aql 1982, Snijders et al. 1987, Andreä et al. 1994; QU Vul 1984, Andreä et al. 1994), sulfur (Nova Aql 1982, Snijders et al. 1987, Andreä et al. 1994), chlorine (Nova GQ Mus 1983, Morisset & Pequignot 1996), argon and calcium (Nova GQ Mus 1983, Morisset & Pequignot 1996; Nova V2214 Oph 1988, Nova V977 Sco 1989 and Nova V443 Sct 1989, Andreä et al. 1994). Indeed, models of explosions in $1.35 M_{\odot}$ ONe white dwarfs have an end-point for nucleosynthesis below calcium, hence in agreement with observations. This suggests that peak temperatures attained at the burning shell during nova outbursts cannot be much larger than 3×10^8 K, otherwise an rp-process would result at such high temperatures, driving the nuclear path towards heavier species, not observed so far. Moreover, as stated in the discussion of the main nuclear paths, determination of chemical abundances in the Si–Ca mass region during nova outbursts is affected by uncertainties of nuclear physics origin. In particular, the uncertainty associated to $^{30}\text{P}(\text{p},\gamma)$ makes it difficult to determine realistic abundances above silicon, and to clarify as well whether the path towards heavier species is halted or, on the contrary, if significant production of Si–Ca nuclei is still expected. A better determination of this crucial rate would be of significant importance for the studies of nova nucleosynthesis that takes place in massive ONe white dwarfs.

The authors would like to thank an anonymous referee for his suggestions. This research has been partially supported by the CICYT-P.N.I.E. (ESP98-1348), by the DGICYT (PB97-0983-C03-02; PB97-0983-C03-03), and by the MCYT (AI HF1999-0140).

REFERENCES

- Amari, S., Gao, X., Nittler, L. R., Zinner, E., José, J., Hernanz, M., and Lewis, R. S. 2001, *ApJ*, 551, 1065
- Andreä, J., Drechsel, H., and Starrfield, S. 1994, *Astron. Astrophys.*, 291, 869
- Angulo, C., Arnould, M., Rayet, M., et al., (The NACRE collaboration) 1999, *Nucl. Phys.*, A656, 3
- Angulo, C. 2000, private communication
- Caughlan, G. R., and Fowler, W. A. (CF88) 1988, *ADNDT*, 40, 283
- Clayton, D. D., and Hoyle, F. 1974, *ApJ*, 187, L101
- Coc, A., Porquet, M.-G., and Nowacki, F. 2000a, *Phys. Rev.*, C61, 015801
- Coc, A., Hernanz, M., José, J., and Thibaud, J.P. 2000b, *Astron. Astrophys.*, 357, 561
- Endt, P.M. 1990, *Nucl. Phys.*, A521, 1
- Endt, P.M. 1998, *Nucl. Phys.*, A633, 1
- Gómez-Gomar, J., Hernanz, M., José, J., and Isern, J. 1998, *MNRAS*, 296, 913
- Goriely, S. 1996, *Nucl. Phys.*, A605, 28
- Hernanz, M., José, J., Coc, A., Gómez-Gomar, J., and Isern, J. 1999, *ApJ*, 526, L97
- Herndl, H., Gorres, J., Wiescher, M., Brown, B.A., and Van Wormer, L. 1995, *Phys. Rev.*, C52, 1078
- Iliadis, C., Giesen, U., Gorres, J., et al. 1991, *Nucl. Phys.*, A533, 153
- Iliadis, C. Giesen, U., Gorres, J., et al. 1992, *Nucl. Phys.*, A539, 97
- Iliadis, C. Görres, J., Ross, J.G., et al. 1993, *Nucl. Phys.*, A559, 83
- Iliadis, C., Endt, P.M., Prantzos, N., and Thompson, W.J. 1999, *ApJ*, 524, 434

- Iliadis, C., D’Auria, J.M., Starrfield, S., Thompson, W.J., and Wiescher, M. 2001, *ApJS*, 134, 151
- José, J., and Hernanz, M. 1998, *ApJ*, 494, 680
- José, J., Hernanz, M., and Coc, A. 1997, *ApJ*, 479, L55
- José, J., Coc, A., and Hernanz, M. 1999, *ApJ*, 520, 347
- Kovetz, A., and Prialnik, D. 1997, *ApJ*, 477, 356
- Lefebvre, A., Vouzoukas, S., Aguer P. et al., 1997, *Nucl. Phys.*, A621, 199c [Errata in 1998, *Nucl. Phys.*, A628, 686]
- Leising, M. D., and Clayton, D. D. 1987, *ApJ*, 323, 159
- Morisset, C., and Pequignot, D. 1996, *Astron. Astrophys.*, 312, 135
- Politano, M., Starrfield, S., Truran, J. W., Weiss, A., and Sparks W. M. 1995, *ApJ*, 448, 807
- Ritossa, C., García-Berro, E., and Iben, I. 1996, *ApJ*, 360, 489
- Romano, D., Matteucci, F., Molaro, P., and Bonifacio, P. 1999, *Astron. Astrophys.*, 352, 117
- Ross, J.G. Görres, J. Iliadis, C. et al. 1995, *Phys. Rev.*, C52, 1681
- Snijders, M. A. J., Batt, T. J., Roche, P. F., Seaton, M. J., Spoelstra, T. A. T., and Blades, J.V C. 1987, *MNRAS*, 228, 329
- Starrfield, S., Truran, J. W., Sparks, W. M., and Arnould, M. 1978, *ApJ*, 222, 600
- Starrfield, S., Gehrz, R. D., and Truran, J. W. 1997, *Astrophysical implications of the laboratory study of presolar materials*, T. Bernatowicz and E. Zinner, New York: AIP, 203
- Starrfield, S., Truran, J. W., Wiescher, M. C., and Sparks, W. M. 1998, *MNRAS*, 296, 502
- Starrfield, S., Iliadis, C., Truran, J. W., Wiescher, M., and Sparks, W. M. 2001, *Nucl. Phys.*, A688, 110
- Thielemann, F.-K., Arnould, M., and Truran, J. W. (SMOKER) 1987, *Advances in Nuclear Astrophysics*, E. Vangioni-Flam, Gif sur Yvette: Editions Frontière, 525
- Thompson, W. J., and Iliadis, C. 1999, *Nucl. Phys.*, A647, 259

Vanlandingham, K. M., Starrfield, S., Wagner, R. M., Shore, S. N., and Sonneborn, G. 1996, MNRAS, 282, 563

Vanlandingham, K. M., Starrfield, S., and Shore, S.N. 1997, MNRAS, 290, 87

Van Wormer, L., Görres, J., Iliadis, C., Wiescher, M., and Thielemann, F.-K. 1994, ApJ, 432, 326

Vouzoukas, S., Browne, C.P., Giesen, U., et al. 1994, Phys. Rev., C50, 1185

Wanajo, S., Hashimoto, M., and Nomoto, K. 1999, ApJ, 523, 409

Wiescher, M., and Görres, J. 1988, Zeit. Phys., A329, 121

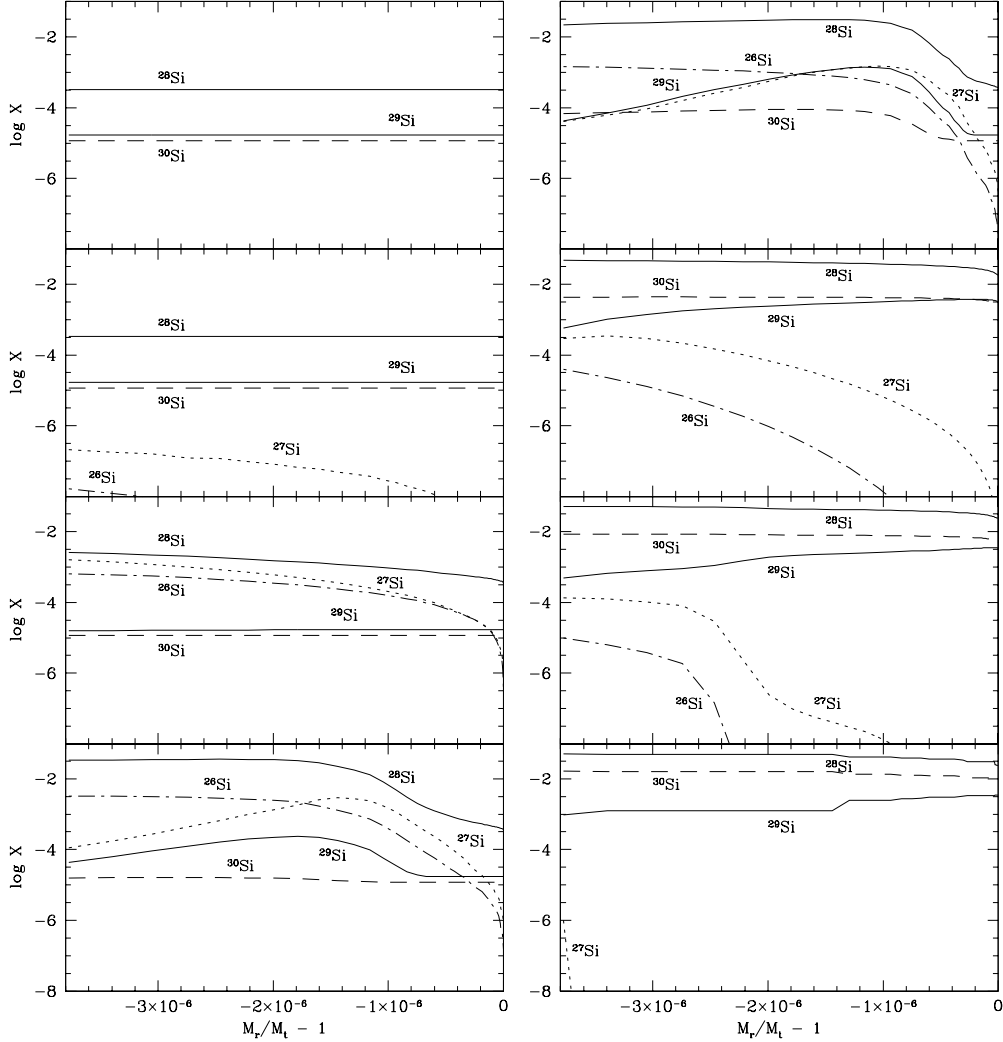


Fig. 2.— Snapshots of the evolution of silicon isotopes (in mass fractions) along the accreted envelope, for a $1.35 M_{\odot}$ One nova accreting at a rate of $\dot{M} = 2 \times 10^{-10} M_{\odot} \cdot \text{yr}^{-1}$. The mass coordinate represents the mass below the surface relative to the total mass. From top to bottom, panels correspond to the time for which the temperature at the burning shell reaches 8×10^7 , 10^8 , 2×10^8 , 3×10^8 , and $T_{peak} = 3.26 \times 10^8$ K, plus three panels corresponding to the last phases of the explosion, when the white dwarf envelope has already expanded to a size of $R_{wd} \sim 10^9$, 10^{10} , and 10^{12} cm, respectively. The base of the ejected shells correspond to a mass coordinate of -3.05×10^{-6} .

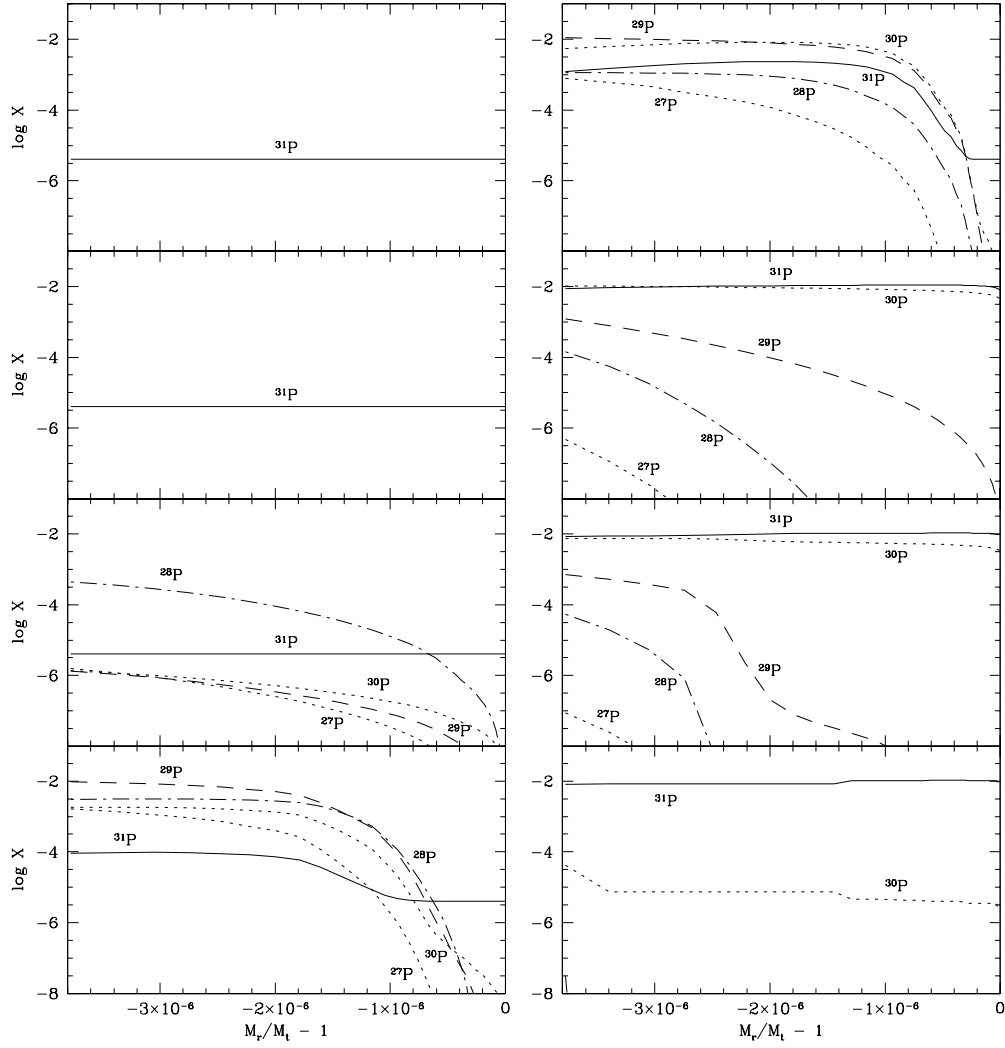


Fig. 3.— Same as Fig. 2, for phosphorus isotopes.

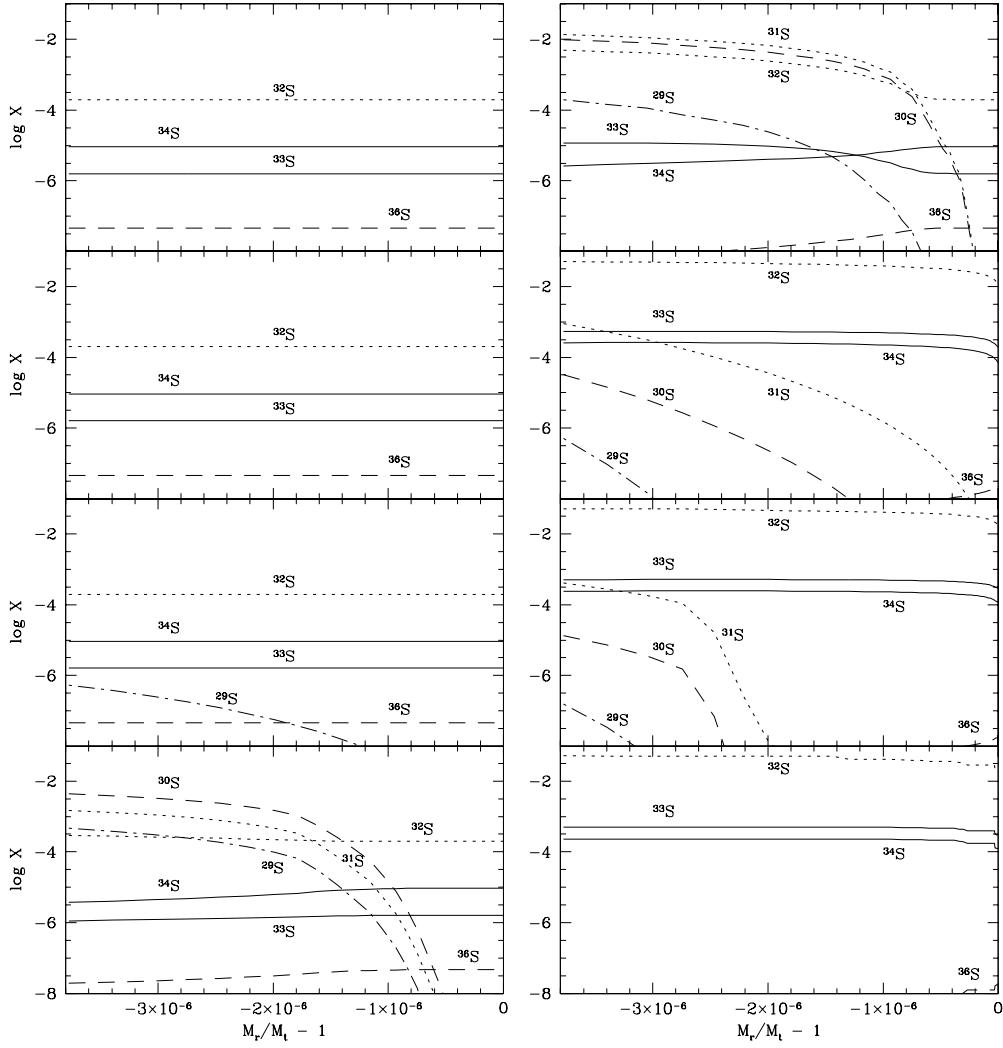


Fig. 4.— Same as Fig. 2, for sulfur isotopes.

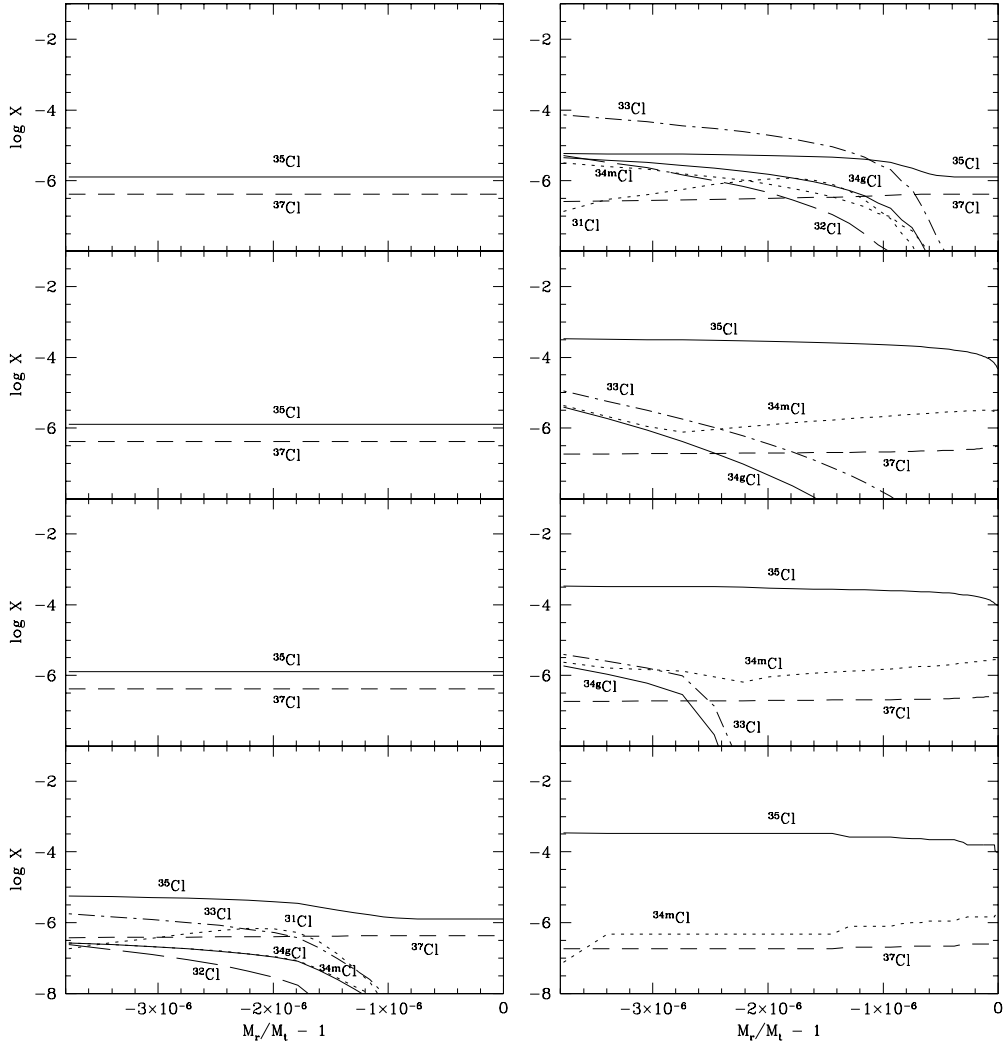


Fig. 5.— Same as Fig. 2, for chlorine isotopes.

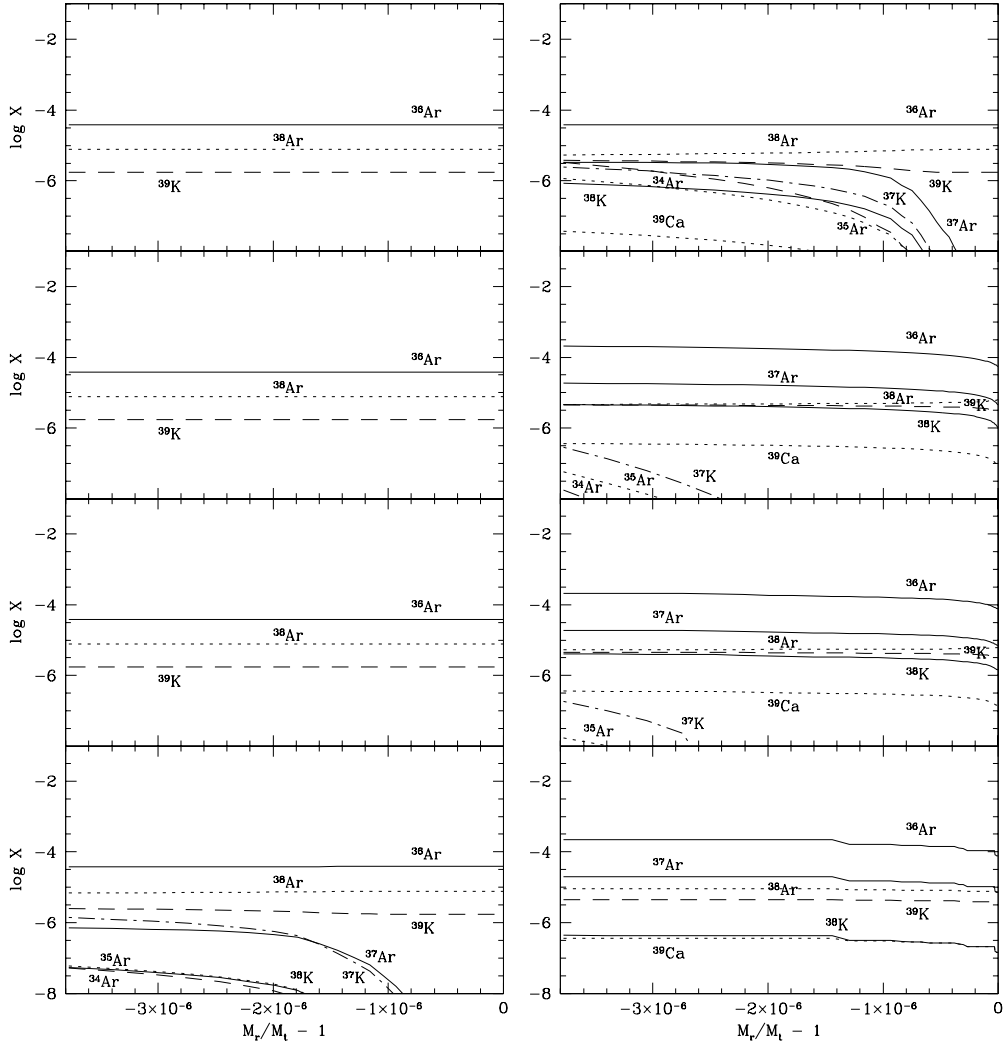


Fig. 6.— Same as Fig. 2, for argon, potassium and calcium isotopes.

Table 1: Initial composition (Si to Ca) in the accreted envelope, assuming a 50% degree of mixing with the ONe white dwarf core (see Ritossa et al. 1996).

Nuclei	Mass fraction
²⁸ Si	3.3E-4
²⁹ Si	1.7E-5
³⁰ Si	1.2E-5
³¹ P	4.1E-6
³² S	2.0E-4
³³ S	1.6E-6
³⁴ S	9.3E-6
³⁶ S	4.7E-8
³⁵ Cl	1.3E-6
³⁷ Cl	4.3E-7
³⁶ Ar	3.9E-5
³⁸ Ar	7.7E-6
³⁹ K	1.7E-6

Table 2: Mean composition of the ejecta (Si to Ca) from 1.35 M_{\odot} ONe white dwarf models. Solar values are given for comparison.

Nuclei	Solar	Model ONe135B	Model p30low	Model 135nom	Model p30high
^{28}Si	6.5E-4	4.2E-2	3.9E-2	4.4E-2	4.5E-2
^{29}Si	3.5E-5	2.1E-3	1.9E-3	1.9E-3	1.9E-3
^{30}Si	2.4E-5	1.4E-2	6.8E-2	1.4E-2	4.6E-4
^{31}P	8.2E-6	8.4E-3	1.1E-3	9.3E-3	1.2E-2
^{32}S	4.0E-4	2.3E-2	4.6E-3	4.5E-2	5.5E-2
^{33}S	3.3E-6	7.6E-3	4.6E-5	4.8E-4	5.9E-4
^{34}S	1.9E-5	9.3E-3	2.2E-5	2.2E-4	2.7E-4
^{36}S	6.4E-8	6.6E-9	5.6E-9	6.0E-9	6.1E-9
^{35}Cl	3.5E-6	4.5E-3	2.9E-5	2.9E-4	3.6E-4
^{37}Cl	1.2E-6	1.4E-4	9.0E-6	1.7E-5	2.0E-5
^{36}Ar	7.7E-5	2.2E-3	5.1E-5	1.9E-4	2.3E-4
^{38}Ar	1.5E-5	2.7E-5	8.1E-6	9.1E-6	9.5E-6
^{39}K	3.5E-6	5.2E-6	4.8E-6	4.7E-6	4.7E-6